

Fabry-Pérot nanocavities controlled by Casimir forces in electrolyte solutions

Lixin Ge^{1,*}, Kaipeng Liu,¹ Ke Gong,¹ and Rudolf Podgornik^{2,3,4,†}

¹School of Physics and Electronic Engineering, Xinyang Normal University, Xinyang 464000, China

²School of Physical Sciences and Kavli Institute of Theoretical Science, University of Chinese Academy of Sciences, Beijing 100049, China

³CAS Key Laboratory of Soft Matter Physics, Institute of Physics, Chinese Academy of Sciences, Beijing 100090, China

⁴Wenzhou Institute of the University of Chinese Academy of Sciences, Wenzhou, Zhejiang 325011, China

(Received 12 December 2023; revised 19 February 2024; accepted 1 April 2024; published 22 April 2024)

We propose a design for tuning the resonant spectra of Fabry-Pérot nanocavities mediated by the Casimir force. The system involves a suspended gold nanoplate approaching a dielectric-coated gold substrate in a univalent electrolyte solution. The gold nanoplate can be stably suspended due to the delicate balance between repulsive and attractive components of the Casimir forces. In an electrolyte solution, the presence of ionic-charge fluctuations can partially or totally screen the thermal $n = 0$ Matsubara term, resulting in strongly modified interactions. As a result, the separation between the gold nanoplate and the substrate experiences a significant modulation in response to variations in salt concentration. Under proper conditions, we find that the modulation of the Casimir force would strongly shift the resonances of Fabry-Pérot nanocavities at the optical frequencies, when the Debye length of the electrolyte decreases from 1000 nm to 10 nm. Finally, the temperature dependence of the thermal Casimir force would provide an additional modulation of Fabry-Pérot nanocavity resonances for their eventual fine tuning. These results open up a promising venue for general tuning of the optical resonances with potential applications in reconfigurable microfluidic nanophotonics.

DOI: 10.1103/PhysRevApplied.21.044040

I. INTRODUCTION

The Fabry-Pérot (F-P) cavity (also referred to as the Fabry-Pérot interferometer), being a basic element of optical spectroscopy, is of great importance in various applications as, e.g., in atomic spectroscopy, metrology, and miscellaneous devices [1]. At micro/nanoscales, the F-P nanocavity consisting of a metal-insulator-metal (MIM) sequence has received considerable attention [2–7], because such simple nanocavities can provide strong light-matter interactions in nanophotonics. In general, the resonances of the F-P nanocavities are fixed once they are fabricated, but can be tuned by changing the cavity size or the refractive index of the intervening medium, e.g., by a static control of the F-P cavity via an inserted plasmonic metasurface with a resonance at visible frequencies [7]. Achieving the dynamic control of the F-P cavity *in situ* is more challenging. Some progress was achieved based on the nonlinear response of the epsilon-near-zero (ENZ) medium at the infrared frequencies [7], but in general it is difficult to change the refractive index dynamically in

the visible frequencies regime. Therefore, the dynamic tuning of F-P nanocavities at visible frequencies remains an interesting open problem.

Recently, a new concept for tunable F-P nanocavities mediated by Casimir forces has been proposed by Esteso et al. [8,9]. The “Casimir force” as used in this paper, within the confines of the Lifshitz theory of van der Waals interactions [10], refers to a macroscopic electromagnetic fluctuation effect with zero-point energy [11] as well as thermal fluctuation contributions [12]. In most cases, the Casimir forces between two macroscopic metallic surfaces in vacuum are attractive (see, e.g., the experiments [13–15] and recent reviews [16,17]), but interestingly, the Casimir forces between two dielectric bodies separated by a liquid layer can be repulsive, when the permittivity of the intervening liquid is higher than one of but smaller than the other of the two interacting dielectrics over a sufficiently wide range of frequencies [18,19]. The balance between repulsive and attractive Casimir forces gives rise to stable Casimir suspensions in different configurations [20–25]. The suspension due to the Casimir forces are generally in the range of hundreds of nanometers, which of course is highly relevant for designing nanocavities.

The Casimir interactions in electrolyte solutions has received considerable attention over the years [16,26–32].

*Corresponding author: lixinge@hotmail.com

†Corresponding author: podgornikrudolf@ucas.ac.cn

The consensus view is that the Casimir interactions with nonzero ($n > 0$) Matsubara frequencies are not affected by the presence of electrolyte ions, but the zero-frequency (thermal) component, i.e., the $n = 0$ Matsubara term, is modulated due to the screening effect stemming from the charge fluctuations of the electrolyte ions [29]. Recently, the screening of the Casimir interaction between two silica microspheres has been detected experimentally by optical tweezers [32].

Here, we propose a design to tune the resonances of F-P nanocavities mediated by the Casimir forces in a univalent electrolyte solution. The system consists of a suspended gold nanoplate adjacent to a gold substrate with dielectric coatings. The gold nanoplate can be stably suspended due to the finely tuned balance between repulsive and attractive Casimir forces and the suspension height can be modulated strongly via the electrolyte concentration, stemming from the partially or completely screened $n = 0$ Matsubara term. We find that the shifting of the resonant spectrum of the F-P nanocavities at the visible frequencies would result in tens of nanometers. Finally, as the Debye length decreases, we find that the thermal Casimir effect modulation of the resonances is suppressed significantly. This work proposes a new scheme for tuning and controlling the optical resonances, which may find application in microfluidic nanophotonics, such as active optical filters, sensors, and others.

II. THEORETICAL MODELS

The F-P nanocavity geometry is shown schematically in Fig. 1. Light is incident from the top, and the two parallel mirrors consist of the gold nanoplate and the gold substrate with different coatings. The gold nanoplate with thickness $L_0 = 40$ nm is suspended within a univalent electrolyte solution, and its separation from the substrate is denoted by d . For calculational simplicity the gold nanoplate is considered as a semi-infinite slab since its in-plane dimension (e.g., about 20 μm), greatly exceeds the separation d . In the absence of ionic-charge fluctuations, the Casimir pressure between the nanoplate and the substrate can be derived within the Lifshitz theory as [15,16]

$$P_c(d) = -\frac{k_B T}{\pi} \sum_{n=0}^{\infty}' \int_0^{\infty} k_{\parallel} K dk_{\parallel} \sum_{\alpha} \frac{r_t^{\alpha} r_b^{\alpha} e^{-2Kd}}{1 - r_t^{\alpha} r_b^{\alpha} e^{-2Kd}}, \quad (1)$$

where k_B is Boltzmann's constant, T is the temperature of the system, the prime in summation denotes a prefactor 1/2 for the term $n = 0$, k_{\parallel} is the parallel wavevector projecting onto the surface plane of the plates, $K = \sqrt{k_{\parallel}^2 + \epsilon_{liq}(i\xi_n)\xi_n^2/c^2}$ is the vertical wavevector, c is the speed of light in vacuum, and $\epsilon_{liq}(i\xi_n)$ is the permittivity of the liquid evaluated by the discrete imaginary Matsubara frequencies, $\xi_n = 2\pi(k_b T/\hbar)n$ ($n = 0, 1, 2 \dots$), with

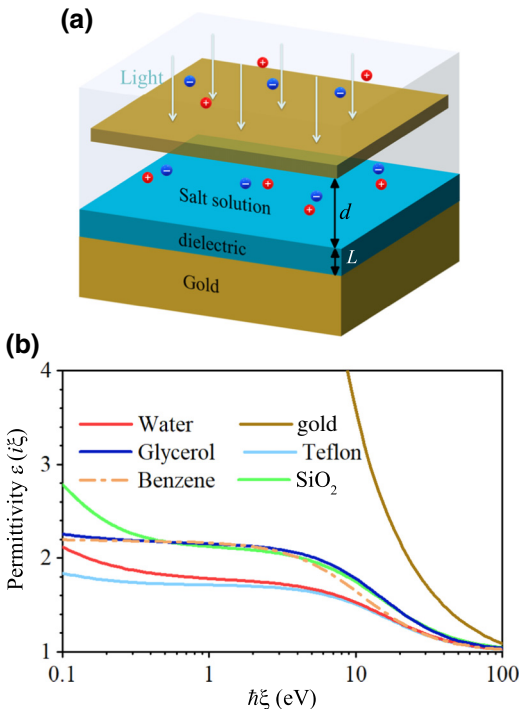


FIG. 1. (a) Schematic view of the Fabry-Pérot nanocavity composed of a gold substrate with a dielectric coatings, and a gold nanoplate, separated by an intervening electrolyte solution with a separation d . The thicknesses of the dielectric coating and the gold nanoplate are L and L_0 , respectively. (b) The dielectric permittivity of the materials constituting the nanocavity, evaluated at imaginary frequencies.

\hbar being the Plank's constant. The $n = 0$ term refers to thermal fluctuations, whereas the rest of the sum refers to quantum fluctuations. r_j^{α} ($j = t, b$; $\alpha = \text{TE}, \text{TM}$) is the reflection coefficient, the subscripts t and b represent the reflection for the top and bottom layered structures, and the superscripts $\alpha = \text{TE}$ and TM represent the polarizations of transverse electric (TE) and transverse magnetic (TM) modes, respectively. The reflection coefficients for a nanofilm can be obtained analytically as [33]

$$r^{\alpha} = \frac{r_{12}^{\alpha} + r_{23}^{\alpha} e^{-2k_z L}}{1 + r_{12}^{\alpha} r_{23}^{\alpha} e^{-2k_z L}}, \quad (2)$$

where L denotes the thickness of the coating, and we have

$$r_{12}^{\text{TM}} = \frac{\epsilon_2(i\xi_n)k_{1z}(i\xi_n, k_{\parallel}) - \epsilon_1(i\xi_n)k_{2z}(i\xi_n, k_{\parallel})}{\epsilon_2(i\xi_n)k_{1z}(i\xi_n, k_{\parallel}) + \epsilon_1(i\xi_n)k_{2z}(i\xi_n, k_{\parallel})}, \quad (3)$$

$$r_{12}^{\text{TE}} = \frac{k_{1z}(i\xi_n, k_{\parallel}) - k_{2z}(i\xi_n, k_{\parallel})}{k_{1z}(i\xi_n, k_{\parallel}) + k_{2z}(i\xi_n, k_{\parallel})}, \quad (4)$$

$$r_{23}^{\text{TM}} = \frac{\epsilon_3(i\xi_n)k_{2z}(i\xi_n, k_{\parallel}) - \epsilon_2(i\xi_n)k_{3z}(i\xi_n, k_{\parallel})}{\epsilon_3(i\xi_n)k_{2z}(i\xi_n, k_{\parallel}) + \epsilon_2(i\xi_n)k_{3z}(i\xi_n, k_{\parallel})}, \quad (5)$$

$$r_{23}^{\text{TE}} = \frac{k_{2z}(i\xi_n, k_{\parallel}) - k_{3z}(i\xi_n, k_{\parallel})}{k_{2z}(i\xi_n, k_{\parallel}) + k_{3z}(i\xi_n, k_{\parallel})}, \quad (6)$$

where $k_{jz} = \sqrt{k_{\parallel}^2 + \epsilon_j(i\xi_n)\xi_n^2/c^2}$ ($j = 1, 2, 3$) is the vertical wavevector in medium j , the subscripts of r_{12}^{α} represent the light is incident from medium 1 to medium 2. Note that this way of subscript indication is also applied to the reflection coefficient r_{23}^{α} . For the suspended gold nanoplate immersed in a liquid, media 1 and 3 are both liquids, whereas medium 2 is gold. For a dielectric-coated gold substrate, media 1, 2, and 3 are the liquid, dielectric, and gold, respectively. Alternatively, the reflection coefficients for layered structures can be calculated using a transfer matrix method [34].

For the $n = 0$ Matsubara term, the reflection coefficients for the TE modes are zero. Consequently, the Casimir pressure is a consequence of the TM mode only. Moreover, the presence of mobile ions modifying the charge fluctuations in the electrolyte solution necessarily implies ionic screening and the $n = 0$ Matsubara term is modified, assuming the form [10]

$$P_c(d)|_{n=0} = -\frac{k_B T}{2\pi} \int_0^{\infty} k_{\parallel} \bar{K} dk_{\parallel} \frac{\bar{r}_t^{\text{TM}} \bar{r}_b^{\text{TM}} e^{-2\bar{K}d}}{1 - \bar{r}_t^{\text{TM}} \bar{r}_b^{\text{TM}} e^{-2\bar{K}d}}. \quad (7)$$

The bar on the symbol means the modification due to ionic-charge fluctuations in the solution. The vertical wavevector in the intervening liquid becomes $\bar{K} = \sqrt{k_{\parallel}^2 + \kappa^2}$, where $\kappa = 1/\lambda_D$, and λ_D is the Debye screening length in the electrolyte solution, defined as

$$\lambda_D = \sqrt{\frac{\epsilon \epsilon_0 k_B T}{e^2 \sum_v n_v v^2}}, \quad (8)$$

where n_v is the number density of ions of valency v in the electrolyte solution, ϵ is the static permittivity of solution, and ϵ_0 is the permittivity of vacuum. Here, we only consider the univalent electrolyte and $v = 1$. In the limit $\kappa \rightarrow 0$, the Casimir pressure in Eq. (7) reduces to the conventional one, and the effect of ionic screening is negligible. If the Debye length is comparable to or even smaller than the separation, the screening has a substantial effect on the $n = 0$ term and can effectively quench it.

Given the high permittivity of gold at zero frequency, the reflection coefficient for the suspended gold nanoplate can be approximated as $\bar{r}_t^{\text{TM}} = 1$. For the dielectric-coated gold substrate, the reflection coefficient becomes

$$\bar{r}_b^{\text{TM}} = \frac{\bar{r}_{12}^{\text{TM}} + e^{-2k_{2z}L}}{1 + \bar{r}_{12}^{\text{TM}} e^{-2k_{2z}L}}, \quad (9)$$

where

$$\bar{r}_{12}^{\text{TM}} = \frac{\epsilon_2 \bar{k}_{1z}(k_{\parallel}, \kappa) - \epsilon_1 \bar{k}_{2z}(k_{\parallel})}{\epsilon_2 \bar{k}_{1z}(k_{\parallel}, \kappa) + \epsilon_1 \bar{k}_{2z}(k_{\parallel})}, \quad (10)$$

and $\bar{k}_{1z}(k_{\parallel}, \kappa) = \sqrt{k_{\parallel}^2 + \kappa^2}$, $\bar{k}_{2z}(k_{\parallel}) = k_{\parallel}$, ϵ_1 , and ϵ_2 are the static permittivities of the liquid and the dielectric layer, respectively. When the static permittivity of the intervening solution is much larger than that of the dielectric coating (i.e., $\epsilon_1 \gg \epsilon_2$), we have $\bar{r}_{12}^{\text{TM}} \approx -1$ at the limit $\kappa \rightarrow 0$. Then, the Casimir pressure in Eq. (7) can be written in an explicit analytical form:

$$P_c(d)|_{n=0} = \frac{3k_B T \zeta(3)}{32\pi d^3}, \quad (11)$$

where $\zeta(x)$ is the Riemann zeta function. The Casimir pressure generated by the $n = 0$ term is always repulsive when the ionic-charge fluctuations are negligible. As κ increases, the reflection coefficient \bar{r}_{12}^{TM} would go from -1 to 1 , gradually changing Casimir interaction of the $n = 0$ term from repulsion to attraction. Most importantly, the magnitude of the phase $e^{-2\bar{K}d}$ in Eq. (7) decreases and eventually approaches zero. As a result, the Casimir pressure contributed from the $n = 0$ term will vanish, as a consequence of the ionic screening effect.

III. RESULTS AND DISCUSSION

The frequency-dependent dielectric functions of the materials are very important for the computations of reflection coefficients and consequently for the evaluation of the Casimir pressure. Here, the generalized Drude-Lorentz model is applied to characterize the dielectric behavior of gold [35]. The dielectric permittivities of silica (SiO_2), Teflon, glycerol, benzene, and water are adopted from recent literature [36], taking into account electronic degrees of freedom as well as the optical bandgap. Figure 1(b) shows the dielectric permittivity of applied materials evaluated at imaginary frequency. The energy for the Matsubara term $n = 1$ is about 0.16 eV at room temperature $T = 300$ K. For Matsubara terms $n \geq 1$, Teflon exhibits the lowest permittivity, whereas gold displays the highest. The dielectric permittivity of water is close to that of Teflon, and smaller than that of SiO_2 , whereas the dielectric responses of glycerol and benzene are similar to that of SiO_2 . We note that the static permittivities of water (~ 78) and glycerol (~ 42) are significantly larger than those of Teflon (~ 2.0) and silica (~ 3.9). On the other hand, the static permittivity of benzene is similar to that of Teflon. The gold surfaces and the dielectric coatings are assumed to be uncharged and consequently the electrostatic interactions are not considered explicitly. We discuss this assumption in more detail later on.

We specifically consider two types of dielectric coatings, namely Teflon and silica. In Fig. 2, we present the decomposition of the Casimir pressure, neglecting the ionic screening effect at $n = 0$ term. The Casimir pressure stemming from the $n = 0$ term exhibits a long-range repulsion for the case of water@Teflon, shown in Fig. 2(a).

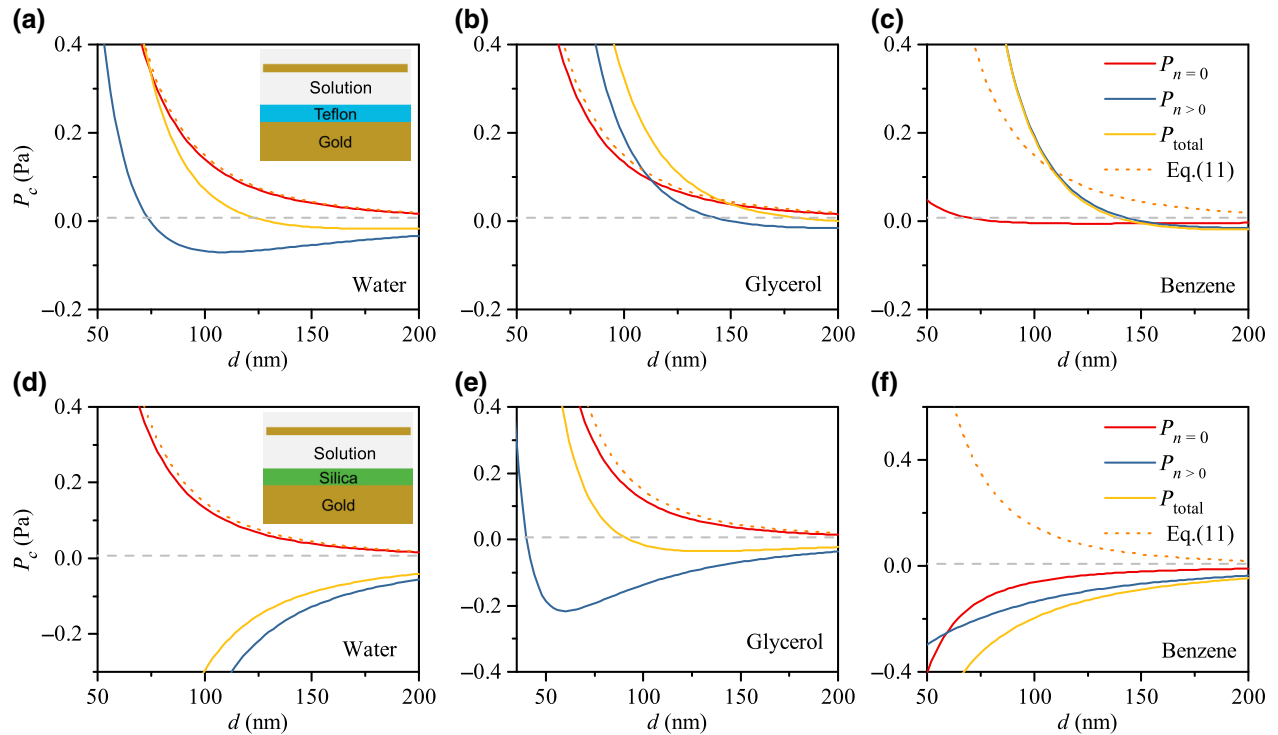


FIG. 2. Decomposition of the Casimir pressure as a function of separation in different electrolyte solutions. The positive (negative) pressure values denote repulsive (attractive) forces. The gray dashed lines represent the magnitude of pressure arising from gravity and buoyancy. The orange dot lines represent the Casimir pressure stemming from the $n = 0$ Matsubara term, computed using the analytical form of Eq. (11). Panels (a)–(c) and (d)–(f) show the Casimir pressure when Teflon and silica are the respective dielectric coatings. The coating layer thickness is fixed at $L = 150$ nm, and the temperature $T = 300$ K.

As expected, the analytical result derived from Eq. (11) is close to the comprehensive numerical result for $n = 0$ term. The contributions from higher-order $n > 0$ terms results in a repulsive force at short separations, transitioning to an attractive force at larger separations. Evidently, the influence of the $n = 0$ term plays a pivotal role in the overall Casimir pressure and this dominance can be attributed to the high contrast of static dielectric permittivities of water and Teflon. The total Casimir force would be significantly altered if the $n = 0$ term is screened by the ionic-charge fluctuations.

In the case of silica as the coating dielectric, the contribution from $n = 0$ remains long-range and repulsive, as depicted in Fig. 2(d). Comparatively, there is a slight increase in the deviation between the numerical calculations and the analytical form of Eq. (11), when contrasted with the Teflon coating configuration. This discrepancy arises from the fact that the static permittivity of silica is larger than that of Teflon. With silica coating, contributions from the $n > 0$ terms exhibit an attractive force, being larger than the $n = 0$ term. Consequently, the total Casimir pressure is long-range attractive, precluding a stable Casimir trapping. This implies that the water@silica coating setup may not be suitable for achieving a tunable F-P cavity. Note that the dielectric coating layer is

necessary to manifest the role of the $n = 0$ term. For $L = 0$ nm, the contribution from the $n = 0$ term becomes secondary even in the case when the solutions are water and glycerol.

The Casimir pressure for the glycerol solution is presented in both Figs. 2(b) and 2(e), where the dielectric layers are Teflon and silica, respectively. In both configurations, the Casimir pressure stemming from the $n = 0$ term is important, and the stable suspension is achievable. Hence, glycerol would be a promising candidate for designing tunable F-P nanocavities via a manipulation of the electrolyte concentration. In particular, in the case of glycerol@silica, the $n = 0$ term can be dominant at certain separations, presenting an excellent opportunity for tuning the Casimir pressure via the screening effect.

Let us consider the opposite scenario next. For the benzene@Teflon, the contribution to the Casimir pressure from the $n = 0$ Matsubara term are small, compared with those of the $n > 0$ terms. This is because the static permittivity of benzene and Teflon are close. Yet, a stable Casimir trapping can be found in Fig. 2(c), since the permittivity of benzene is larger than of Teflon for $n > 0$. Due to the weak Casimir pressure stemming from the $n = 0$ term, it would be in this case ineffective to tune the Casimir force via the ionic screening effect. When the dielectric coating is silica,

the Casimir pressures generated from the $n = 0$ and $n > 0$ terms are long-range attractive as shown in Fig. 2(f) and consequently there is no stable suspension, precluding a realization of tunable F-P nanocavities.

Based on the above discussions, the combinations of water@Teflon, glycerol@Teflon, and glycerol@silica, allow for stable suspension resulting in the Casimir force, and the $n = 0$ Matsubara term plays a pivoting role in the total Casimir pressure. This suggests that in these three combinations, effective modulation of the $n = 0$ term can be controlled through adjustments in ion concentration of the electrolyte solution, allowing for a precise control of suspension spacings. In addition, the pressure generated from the sum of gravity and buoyancy should also be considered, which is about 7.0 mPa for $L_0 = 40$ nm [34]. The counterbalance between the Casimir force, gravity and buoyancy produces the total zero force at the equilibrium separation, i.e., d_e . Figure 3(a) illustrates the Casimir pressure at different Debye screening lengths for the case of water@Teflon. When the Debye length $\lambda_D = 10$ nm, the d_e is around 73 nm, with the $n = 0$ term completely screened, and the Casimir force primarily stemming from the $n > 0$ terms. When λ_D is comparable to d_e , e.g., $\lambda_D = 50$ nm and 100 nm, the Casimir force exhibits a stronger repulsion,

resulting in a corresponding increase of d_e . As λ_D increases further to 200 nm and 800 nm, the screening effect is gradually weakened. For the glycerol@Silica combination, we observe a similar behavior where increasing λ_D leads to a gradual increase of the d_e from about 40 to 90 nm [see Fig. 3(b)].

Modulating the ionic concentration can be easily achieved experimentally. For pure water, the Debye screening length is about 1000 nm at room temperature, resulting from the dissociation of the H_2O molecule into the H^+ and OH^- ions. However, when it is exposed to air, the Debye screening length of water decreases from ~ 1000 nm to around 220 nm as the CO_2 in the air dissolves in water (pH around 5.7) [37]. The relationship between the Debye length and the added electrolyte concentration is shown in Fig. 3(c) for the temperature $T = 300$ K and univalent ions ($v = 1$) as in, e.g., NaCl salt solution. As the effective ion concentration increases from 10^{-7} M to 10^{-3} M, the Debye length correspondingly decreases from approximately 1000 nm to 10 nm. Due to the lower solvent static dielectric constant of glycerol compared to water, λ_D in a glycerol solution is slightly lower than that of the aqueous solution with the same salt concentration.

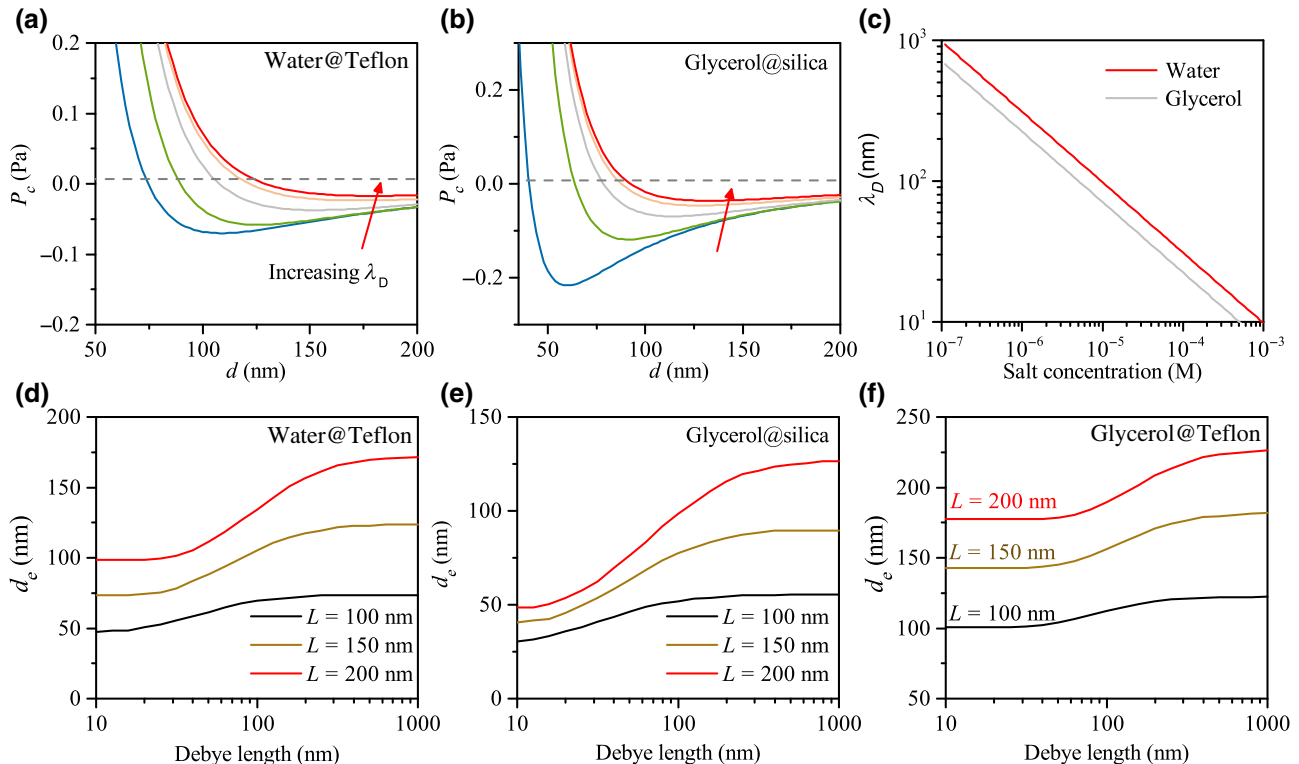


FIG. 3. Casimir pressure as a function of separation under different Debye screening lengths. In panels (a),(b) the Debye screening length λ_D has a sequence: 10, 50, 100, 200, and 800 nm. The electrolyte solution and the dielectric coating are: (a) water@Teflon and (b) glycerol@silica. The gray dashed lines represent the pressure magnitude due to the gravity and buoyancy. (c) Debye screening length versus salt concentration is shown in the log-log plot. (d)–(f) The variation of the equilibrium separation of the gold nanoplate as a function of the Debye screening length for different coating thicknesses L . Here, the temperature $T = 300$ K.

The cavity dimension is a critical parameter for the optical resonance in F-P nanocavities, and it depends on both the dielectric-coating thickness and the suspension height. Figures 3(d)–3(f) illustrate the equilibrium separation changes as a function of the Debye screening length under different coating thicknesses. With a gradual increase in λ_D from 10 nm to 1000 nm, the value of d_e undergoes a corresponding nonlinear modulation. Taking the thickness of $L = 150$ nm for water@Teflon as an example, d_e remains nearly constant as λ_D increases from 10 nm to 30 nm. However, when λ_D increases further from 30 nm to 200 nm, the modulation effect becomes pronounced. In particular, the suspension is highly sensitive to changes of the Debye screening length at around 100 nm. As λ_D continues to increase from 300 to 1000 nm, d_e remains almost constant, because λ_D is now much larger than d_e , and the screening effect at this separations is negligible. The equilibrium separation increases also for larger coating thicknesses, L , stemming from the repulsive terms in the Casimir interaction.

It is worth noting that the modulation range of d_e for the glycerol@silica is larger than that of glycerol@Teflon. For $L = 150$ nm, the maximum difference of equilibrium separation due to screening for glycerol@silica is 50 nm, whereas for glycerol@Teflon, it is only 30 nm. This is because, for $n > 1$, i.e., at the infrared and visible spectral regions, the refractive index of glycerol is close to that of

silica, making the contribution from the $n = 0$ term more prominent. The control of the equilibrium separation due to the ionic screening effects of the $n = 0$ Matsubara term of the Casimir interaction thus proves to be more effective for the case of glycerol@silica.

Figures 4(a) and 4(b) present contour plots of the reflectance spectrum of the F-P cavity as a function of its equilibrium separation. The reflectance is calculated using the transfer matrix method for the real frequencies [38]. For the water@Teflon combination, as the Debye screening length decreases from 1000 nm to 10 nm, the separation d_e is reduced from 123 nm to 73 nm. Similarly, the equilibrium separation decreases from 90 to 40 nm for the glycerol@silica combination. While the equilibrium separation of glycerol@silica is relatively smaller than that of water@Teflon, the higher refractive index of glycerol@silica in the visible spectrum compensates for its smaller separation. Hence, the reflectance resonance spectra of glycerol@silica as modulated via the Debye screening length closely resemble those of the water@Teflon. For these two configurations, the F-P resonance wavelength is approximately 870 nm for $\lambda_D = 1000$ nm, and as λ_D is reduced to 10 nm, the resonance wavelength shifts to around 730 nm.

The transmission-type F-P resonators are preferred in some configurations. In that case the substrate is a finite-thickness gold film placed on a transparent medium, as

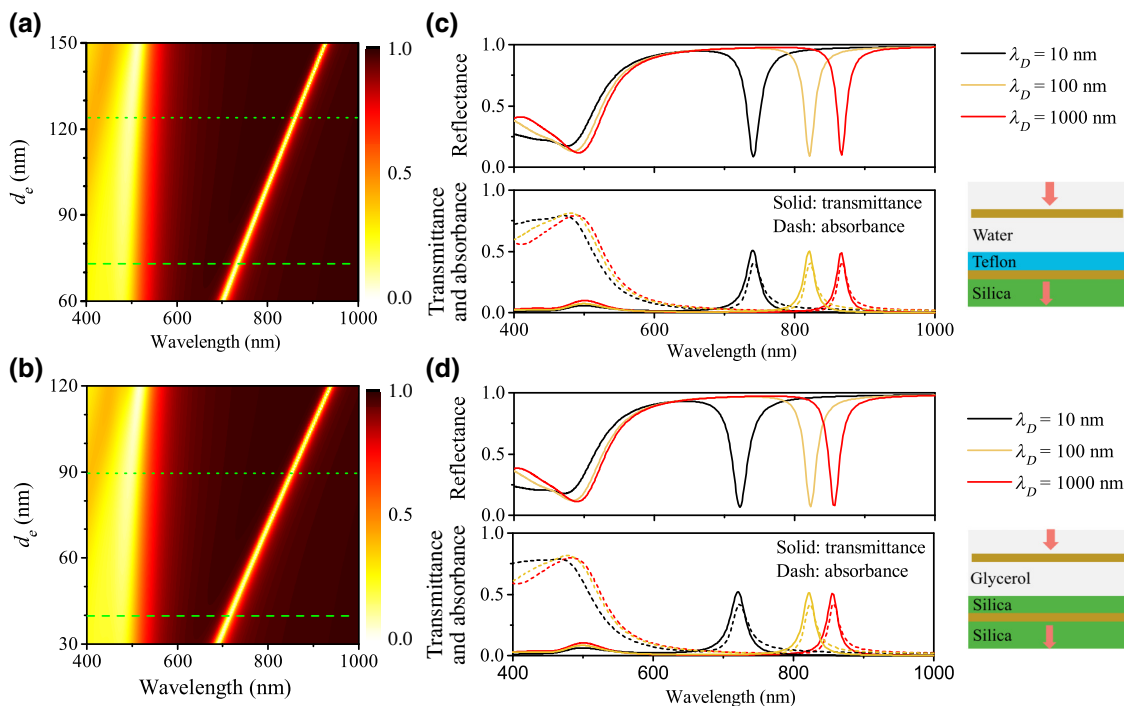


FIG. 4. (a),(b) Reflectance of the F-P nanocavities for different equilibrium separations, where the solution and coating medium consist of water@Teflon and glycerol@silica in (a),(b), respectively. The green dotted and dashed lines correspond to the spectra with Debye screening length being 1000 nm and 10 nm, respectively. (c),(d) Spectra of transmission-type F-P nanocavities, wherein the gold substrate has been replaced by a gold nanofilm deposited on a semi-infinite silica substrate. The thickness of dielectric coating is $L = 150$ nm and the temperature $T = 300$ K.

illustrated in Figs. 4(c) and 4(d). The Casimir force for multilayered substrates remains nearly independent of the gold-film thickness, when the thickness of gold is larger than 20 nm. The reflectance, transmittance, and absorbance are shown in Figs. 4(c) and 4(d) at different Debye screening lengths. The resonance frequencies of transmission-type F-P resonators almost match those of the reflective types. Calculations reveal that the transmittance exceeds 50% at resonance, with an absorbance of about 40%.

The thickness of gold nanofilm (denoted as L'_0) within the multilayer substrate is set to be 40 nm in Figs. 4(c) and 4(d). The Casimir forces between the suspended gold nanoplate and the multilayer substrate are independent of L'_0 when the magnitude of L'_0 is larger than the skin depth (about 22 nm) [39]. On the other hand, the optical responses of the nanocavities, such as the transmittance and quality factor (Q -factor), are closely associated with L'_0 . The transmittance of F-P cavities is decreased (or increased) with increasing (or decreasing) L'_0 , whereas the Q -factor of spectra is enhanced (or reduced) at the same time. Generally, the thickness $L'_0 \sim (30 \text{ nm}, 50 \text{ nm})$ is a good range to design the transmission-type F-P cavities for experiments.

The temperature can also play an important role in the F-P resonators, as reported in our recent work [40]. In a vacuum environment, the contribution of thermal

fluctuation to the Casimir force is comparable to the zero-point energy fluctuation, only at micron separations (e.g., $>3 \mu\text{m}$ at room temperature) [41]. By contrast, the thermal Casimir effect in a liquid environment can be manifested at a submicrometer separation [42,43]. This is because the stable suspensions, attributed to the balance between attractive and repulsive Casimir forces, can easily be disrupted by the change of the temperature. The upper panel in Figure 5 shows the variation of the equilibrium separation under different temperatures. For the configuration of water@Teflon, d_e elevates with increasing temperature, and the variation of d_e is about 15 nm at $\lambda_D = 1000 \text{ nm}$ when the temperature increases from 275 to 350 K, as shown in Fig. 5(a). The temperature-dependent suspension can be suppressed greatly when λ_D declines from 1000 nm to 10 nm. This is because the thermal Casimir effect is mainly attributed to the $n = 0$ term, as reported in [42]. Figures 5(b) and 5(c) show the configurations for glycerol@Teflon and glycerol@silica. The thermal modulation of equilibrium separation for glycerol is much larger than that of water, because the temperature for liquid state of glycerol is much wider(ranging from about 291 to 563 K). When the temperature increases from 300 to 450 K at a fixed $\lambda_D = 1000 \text{ nm}$, the d_e elevates about 30 nm and 35 nm for the systems of glycerol@Teflon and glycerol@silica, respectively. Again, the

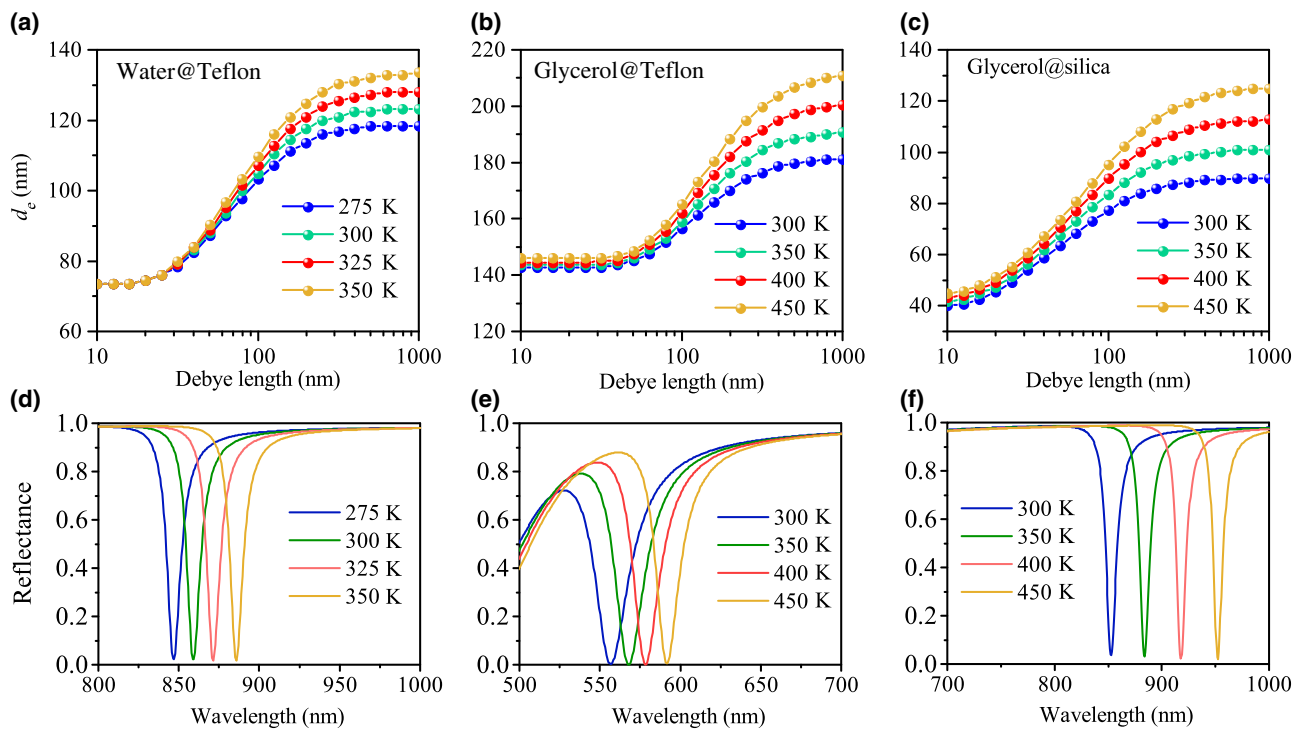


FIG. 5. Equilibrium separation of the gold nanoplate under different temperatures (upper panel). The setup consists of (a) water@Teflon, (b) glycerol@Teflon, and (c) glycerol@silica. The lower panel shows the reflectance spectra of reflection-type F-P cavities under different temperatures, where the Debye length is fixed at 1000 nm. The combinations are (d) water@Teflon, (e) glycerol@Teflon, and (f) glycerol@silica. Here, we set the thickness $L = 150 \text{ nm}$ and $L_0 = 40 \text{ nm}$.

thermal modulations are suppressed greatly, and the deviations of d_e between 300 and 450 K are only $3 \sim 5$ nm as λ_D reduces to 10 nm.

The thermal ($n = 0$) and quantum ($n > 0$) fluctuations are often discussed in terms of the interplay between the separated distance d and the thermal wavelength λ_T [44–46]. In general, the quantum fluctuation is dominant at a small separation, whereas the thermal Casimir effect becomes dominant when $d > \lambda_T$ [47]. Interestingly, the contribution from thermal Casimir effect can be significantly enhanced at smaller separations in low-dimension systems [48–50]. In the system investigated here, the thermal Casimir effect can be dominant for small separations, see, e.g., Figs. 2(a) and 2(e). This is attributed to the high contrast of static permittivity between the aqueous electrolyte solution and the dielectric coating layer. On the other side, the quantum fluctuation for Casimir interaction ($n > 0$) is small, due to the close permittivity between the solution and dielectric coating-dielectric layer at frequencies $n > 0$. Moreover, the reduction of quantum fluctuations near the equilibrium separation comes from the compensation between the repulsive and attractive Casimir components.

Compared with the direct detection of the magnitude of thermal Casimir force [41], the change of equilibrium separation via temperature can be easily detected by optical spectroscopy. To demonstrate this, the reflection spectra of F-P cavities modulated by the thermal Casimir effect are shown in Figs. 5(d)–5(f), where we consider reflection-type F-P cavities. For the water@Teflon, the shifting of the reflection dips is about 40 nm, as the temperature increases from 275 to 350 K [see Fig. 5(d)]. On the other hand, the shifting of the reflection dips is only about 35 nm for glycerol@Teflon when the temperature increases from 300 to 450 K [see Fig. 5(e)]. Remarkably, the reflection dips have a shift over 100 nm for glycerol@silica [see Fig. 5(f)], making it a good condition to detect the thermal Casimir effect at a submicrometer separation. Note that the shifting reflecting dip via the changing of d_e is strongly dependent on the excited mode of F-P cavities. Here, the excited cavity mode for water@Teflon and glycerol@silica is the fundamental mode with $m = 1$, whereas the excited modes is high-order mode with $m = 2$ for glycerol@Teflon. That is why the shifting wavelength for glycerol@silica is much larger than that of glycerol@Teflon, even though they have a close variation of d_e .

Apart from the Casimir interactions, the electrostatic double-layer forces represent the second component of the nanoscale interactions within the standard Deryaguin-Landau-Verwey-Overbeek (DLVO) paradigm [28]. The screening effect for electrostatic double-layer forces is even more pronounced then for the Casimir forces and modulation of the salt concentration can finely tune the balance between repulsive electrostatic double-layer forces and attractive Casimir forces, as has been recently shown

in the case of a stable equilibrium separation for a gold nanoplate in an aqueous solution [26].

In our analysis we did not delve specifically into the effect of electrostatic double-layer interactions, as they are crucially dependent on the dissociated surface charges of the materials involved, i.e., silica, gold, and Teflon, and require separate modeling of the dissociation mechanism. In fact, silica has complicated dissociation properties [51,52] and its surface charge depends strongly on the solution conditions. The same is true for gold surfaces in aqueous solutions where adsorption of solution ions and dielectric image effects modify the effective surface charge [53], whereas Teflon is of course uncharged. Our analysis would thus be strictly valid for Teflon, whereas it would retain its validity near the point of zero charge for silica and gold [54,55]. The proximity to the point of zero charge can be achieved standardly by designing the proper electrolyte solution conditions by tuning not only the salt concentration but also the pH of the intervening solution [56].

IV. CONCLUSIONS

In summary, we have analyzed a multilayered setup with dominant Casimir interactions as can be realized in F-P nanocavities. We have shown that the resonances of F-P nanocavities can be tunable by ionic-charge fluctuations in an aqueous electrolyte solution via the Debye screening length entering the static Matsubara term in the total Casimir interaction pressure. For the combinations of water@Teflon, glycerol@Teflon, and glycerol@silica, a stable equilibrium separation can be achieved, with the $n = 0$ Matsubara term being a leading contribution to the total Casimir pressure. The $n = 0$ Matsubara term can be partially or completely quenched due to the ionic screening as quantified by the Debye screening length of the electrolyte solution. The quenching effect was found to be most pronounced when the Debye length is comparable with the equilibrium separation, strongly affecting the equilibrium separation of the gold nanoplate next to the coated gold substrate. We have also discussed the shift in the resonant spectrum of F-P nanocavities at optical frequencies for equilibrium separation spanning tens of nanometers, and argue that the tunable F-P resonators could be designed in the form of reflection or transmission type, depending on the substrate. Finally, the resonances of F-P nanocavities have been shown to respond strongly also to temperature variation via its role in the thermal Casimir effect, suggesting that the F-P nanocavities could be excellent platforms to detect the thermal Casimir effect at a submicrometer separation. Our findings provide a promising avenue for dynamic control of optical nanocavities, which may have promising applications in microfluidic nanophotonics.

In our work, the radiation pressure is assumed to be negligible for low incident irradiance $I_{\text{inc}} \ll 10^6 \text{ W/m}^2$.

Indeed, light interferometry is standard technique used in surface force experiments but does not play any role there [57]. However, the radiation pressure plays an important role for high-intensity monochromatic lasers [26], and could eventually even lead to complete destruction of the sample.

ACKNOWLEDGMENTS

This work is supported by the National Natural Science Foundation of China (Grant No. 11804288, 61974127), Natural Science Foundation of Henan Province (Grant No. 232300420120), and the Innovation Scientists and Technicians Troop Construction Projects of Henan Province. R.P. acknowledges funding from the Key Project under contract no. 12034019 of the National Natural Science Foundation of China.

- [1] M. Vaughan, *The Fabry-Perot Interferometer: History, Theory, Practice and Applications* (Routledge, New York, 2017).
- [2] Z. Li, J. Liu, L. Feng, Y. Pan, J. Tang, H. Li, G. Cheng, Z. Li, J. Shi, Y. Xu, *et al.*, Monolithic MOF-based metal–insulator–metal resonator for filtering and sensing, *Nano Lett.* **23**, 637 (2023).
- [3] V. Caligiuri, G. Biffi, M. Palei, B. Martín-García, R. D. Pothuraju, Y. Bretonnière, and R. Krahne, Angle and polarization selective spontaneous emission in dye-doped metal/insulator/metal nanocavities, *Adv. Opt. Mater.* **8**, 1901215 (2020).
- [4] H. Deng, Z. Li, L. Stan, D. Rosenmann, D. Czaplewski, J. Gao, and X. Yang, Broadband perfect absorber based on one ultrathin layer of refractory metal, *Opt. Lett.* **40**, 2592 (2015).
- [5] N. Liu, M. Mesch, T. Weiss, M. Hentschel, and H. Giessen, Infrared perfect absorber and its application as plasmonic sensor, *Nano Lett.* **10**, 2342 (2010).
- [6] A. Ghobadi, H. Hajian, B. Butun, and E. Ozbay, Strong light–matter interaction in lithography-free planar metamaterial perfect absorbers, *ACS Photonics* **5**, 4203 (2018).
- [7] J. Kim, E. G. Carnemolla, C. DeVault, A. M. Shaltout, D. Faccio, V. M. Shalaev, A. V. Kildishev, M. Ferrera, and A. Boltasseva, Dynamic control of nanocavities with tunable metal oxides, *Nano Lett.* **18**, 740 (2018).
- [8] V. Esteso, S. Carretero-Palacios, and H. Míguez, Casimir–Lifshitz force based optical resonators, *J. Phys. Chem. Lett.* **10**, 5856 (2019).
- [9] V. Esteso, D. Frustaglia, S. Carretero-Palacios, and H. Míguez, Casimir-Lifshitz optical resonators: a new platform for exploring physics at the nanoscale, *Adv. Phys. Res.* **3**, 2300065 (2023).
- [10] V. A. Parsegian, *Van der Waals Forces: a Handbook for Biologists, Chemists, Engineers, and Physicists* (Cambridge University Press, Cambridge, 2005).
- [11] H. B. G. Casimir, On the attraction between two perfectly conducting plates, *Proc. Kon. Ned. Akad. Wet.* **51**, 793 (1948).
- [12] M. Bordag, U. Mohideen, and V. M. Mostepanenko, New developments in the Casimir effect, *Phys. Rep.* **353**, 1 (2001).
- [13] G. Bressi, G. Carugno, R. Onofrio, and G. Ruoso, Measurement of the Casimir force between parallel metallic surfaces, *Phys. Rev. Lett.* **88**, 041804 (2002).
- [14] J. L. Garrett, D. A. T. Somers, and J. N. Munday, Measurement of the Casimir force between two spheres, *Phys. Rev. Lett.* **120**, 040401 (2018).
- [15] G. L. Klimchitskaya, U. Mohideen, and V. M. Mostepanenko, The Casimir force between real materials: experiment and theory, *Rev. Mod. Phys.* **81**, 1827 (2009).
- [16] L. M. Woods, D. A. R. Dalvit, A. Tkatchenko, P. Rodriguez-Lopez, A. W. Rodriguez, and R. Podgornik, Materials perspective on Casimir and van der Waals interactions, *Rev. Mod. Phys.* **88**, 045003 (2016).
- [17] T. Gong, M. R. Corrado, A. R. Mahbub, C. Shelden, and J. N. Munday, Recent progress in engineering the Casimir effect—applications to nanophotonics, nanomechanics, and chemistry, *Nanophotonics* **10**, 523 (2020).
- [18] J. N. Munday, F. Capasso, and V. A. Parsegian, Measured long-range repulsive Casimir–Lifshitz forces, *Nature* **457**, 170 (2009).
- [19] P. J. van Zwol and G. Palasantzas, Repulsive Casimir forces between solid materials with high-refractive-index intervening liquids, *Phys. Rev. A* **81**, 062502 (2010).
- [20] R. Zhao, L. Li, S. Yang, W. Bao, Y. Xia, P. Ashby, Y. Wang, and X. Zhang, Stable Casimir equilibria and quantum trapping, *Science* **364**, 984 (2019).
- [21] L. Ge, X. Shi, L. Liu, and K. Gong, Gate-tunable Casimir equilibria with transparent conductive oxides, *Phys. Rev. B* **102**, 075428 (2020).
- [22] H. Toyama, T. Ikeda, and H. Iizuka, Dynamic control of Casimir forces on a nanoflake in a liquid through a tunable graphene layer, *Phys. Rev. B* **108**, 245402 (2023).
- [23] Y. Ye, Q. Hu, Q. Zhao, and Y. Meng, Casimir repulsive-attractive transition between liquid-separated dielectric metamaterial and metal, *Phys. Rev. B* **98**, 035410 (2018).
- [24] X. Liu and Z. M. Zhang, Tunable stable levitation based on Casimir interaction between nanostructures, *Phys. Rev. Appl.* **5**, 034004 (2016).
- [25] V. Esteso, S. Carretero-Palacios, and H. Míguez, Nanolevitation phenomena in real plane-parallel systems due to the balance between Casimir and gravity forces, *J. Phys. Chem. C* **119**, 5663 (2015).
- [26] B. Munkhbatai, A. Canales, B. Küçüköz, D. G. Baranov, and T. O. Shegai, Tunable self-assembled Casimir microcavities and polaritons, *Nature* **597**, 214 (2021).
- [27] T. Schoger, B. Spreng, G.-L. Ingold, P. A. MaiaNeto, and S. Reynaud, Universal Casimir interaction between two dielectric spheres in salted water, *Phys. Rev. Lett.* **128**, 230602 (2022).
- [28] R. H. French, V. A. Parsegian, R. Podgornik, R. F. Rajter, A. Jagota, J. Luo, D. Asthagiri, M. K. Chaudhury, Y. M. Chiang, S. Granick, *et al.*, Long range interactions in nanoscale science, *Rev. Mod. Phys.* **82**, 1887 (2010).
- [29] R. R. Netz, Static van der Waals interactions in electrolytes, *Eur. Phys. J. E* **5**, 189 (2001).
- [30] P. A. Maia Neto, F. S. S. Rosa, L. B. Pires, A. B. Moraes, A. Canaguier-Durand, R. Guérout, A. Lambrecht, and S.

- Reynaud, Scattering theory of the screened Casimir interaction in electrolytes, *Eur. Phys. J. D* **73**, 1 (2019).
- [31] R. O. Nunes, B. Spreng, R. de Melo e Souza, G.-L. Ingold, P. A. Maia Neto, and F. S. S. Rosa, The Casimir interaction between spheres immersed in electrolytes, *Universe* **7**, 156 (2021).
- [32] L. B. Pires, D. S. Ether, B. Spreng, G. R. S. Araújo, R. S. Decca, R. S. Dutra, M. Borges, F. S. S. Rosa, G. L. Ingold, M. J. B. Moura, *et al.*, Probing the screening of the Casimir interaction with optical tweezers, *Phys. Rev. Res.* **3**, 033037 (2021).
- [33] R. Zhao, T. Koschny, E. N. Economou, and C. M. Soukoulis, Repulsive Casimir forces with finite-thickness slabs, *Phys. Rev. B* **83**, 075108 (2011).
- [34] L. Ge, X. Shi, Z. Xu, and K. Gong, Tunable Casimir equilibria with phase change materials: from quantum trapping to its release, *Phys. Rev. B* **101**, 104107 (2020).
- [35] H. S. Sehmi, W. Langbein, and E. A. Muljarov, Optimizing the Drude-Lorentz model for material permittivity: method, program, and examples for gold, silver, and copper, *Phys. Rev. B* **95**, 115444 (2017).
- [36] M. Moazzami Gudarzi and S. H. Aboutalebi, Self-consistent dielectric functions of materials: toward accurate computation of Casimir–Van der waals forces, *Sci. Adv.* **7**, eaab2272 (2021).
- [37] Y. Wang, S. R. Narayanan, and W. Wu, Field-assisted splitting of pure water based on deep-sub-Debye-length nanogap electrochemical cells, *ACS Nano* **11**, 8421 (2017).
- [38] T. Zhan, X. Shi, Y. Dai, X. Liu, and J. Zi, Transfer matrix method for optics in graphene layers, *J. Phys. Condens. Matter* **25**, 215301 (2013).
- [39] A. D. Phan, L. M. Woods, D. Drosdoff, I. V. Bondarev, and N. A. Viet, Temperature dependent graphene suspension due to thermal Casimir interaction, *Appl. Phys. Lett.* **101**, 113118 (2012).
- [40] L. Ge, B. Li, H. Luo, and K. Gong, Electrical and thermal control of Fabry-Pérot cavities mediated by Casimir forces, *Phys. Rev. A* **108**, 062814 (2023).
- [41] A. O. Sushkov, W. J. Kim, D. A. R. Dalvit, and S. K. Lamoreaux, Observation of the thermal Casimir force, *Nat. Phys.* **7**, 230 (2011).
- [42] V. Esteso, S. Carretero-Palacios, and H. Míguez, Effect of temperature variations on equilibrium distances in levitating parallel dielectric plates interacting through Casimir forces, *J. Appl. Phys.* **119**, 144301 (2016).
- [43] A. W. Rodriguez, D. Woolf, A. P. McCauley, F. Capasso, J. D. Joannopoulos, and S. G. Johnson, Achieving a strongly temperature-dependent Casimir effect, *Phys. Rev. Lett.* **105**, 060401 (2010).
- [44] M. Brown-Hayes, J. H. Brownell, D. A. R. Dalvit, W. J. Kim, A. Lambrecht, F. C. Lombardo, F. D. Mazzitelli, S. M. Middleman, V. V. Nesvizhevsky, R. Onofrio, and S. Reynaud, Thermal and dissipative effects in Casimir physics, *J. Phys. A Math. Gen.* **39**, 6195 (2006).
- [45] S. Y. Buhmann and S. Scheel, Thermal Casimir versus Casimir-Polder forces: equilibrium and nonequilibrium forces, *Phys. Rev. Lett.* **100**, 253201 (2008).
- [46] V. B. Svetovoy, Evanescent character of the repulsive thermal Casimir force, *Phys. Rev. A* **76**, 062102 (2007).
- [47] M. Bordag, G. L. Klimchitskaya, U. Mohideen, and V. M. Mostepanenko, *Advances in the Casimir Effect* (Oxford University Press, New York, 2009).
- [48] G. L. Klimchitskaya and V. M. Mostepanenko, Origin of large thermal effect in the Casimir interaction between two graphene sheets, *Phys. Rev. B* **91**, 174501 (2015).
- [49] D.-N. Le, P. Rodriguez-Lopez, and L. M. Woods, Dispersive interactions between standard and Dirac materials and the role of dimensionality, *J. Phys. Mater.* **5**, 034001 (2022).
- [50] P. Rodriguez-Lopez, D.-N. Le, I. V. Bondarev, M. Antezza, and L. M. Woods, Giant anisotropy and Casimir phenomena: the case of carbon nanotube metasurfaces, *Phys. Rev. B* **109**, 035422 (2024).
- [51] C. Labbez, B. Jonsson, M. Skarba, and M. Borkovec, Ion–ion correlation and charge reversal at titrating solid interfaces, *Langmuir* **25**, 7209 (2009).
- [52] J. Yang, H. Su, C. Lian, Y. Shang, H. Liu, and J. Wu, Understanding surface charge regulation in silica nanopores, *Phys. Chem. Chem. Phys.* **22**, 15373 (2020).
- [53] R. R. Kumal, T. E. Karam, and L. H. Haber, Determination of the surface charge density of colloidal gold nanoparticles using second harmonic generation, *J. Phys. Chem. C* **119**, 16200 (2015).
- [54] V. M. Mostepanenko, E. N. Velichko, and M. A. Baranov, Role of electromagnetic fluctuations in organic electronics, *J. Electron. Sci. Technol.* **18**, 100023 (2020).
- [55] M. A. Baranov, G. L. Klimchitskaya, V. M. Mostepanenko, and E. N. Velichko, Fluctuation-induced free energy of thin peptide films, *Phys. Rev. E* **99**, 022410 (2019).
- [56] Y. Avni, D. Andelman, and R. Podgornik, Charge regulation with fixed and mobile charged macromolecules, *Curr. Opin. Electrochem.* **13**, 70 (2019).
- [57] J. N. Connor and R. G. Horn, Extending the surface force apparatus capabilities by using white light interferometry in reflection, *Rev. Sci. Instrum.* **74**, 4601 (2003).